7. RESULTS AND DISCUSSION

The rapid use of digital images in textile industry and the necessity to use computer for fast inspection has created the need to automate the process of defect detection. Methods that can accurately identify and detect defects in patterned fabrics is an area of research field that has gained interest only in the past few decades and the field still have various issues that has to be solved. Important of these issues is to improve the accuracy of defect detection, as errors in this stage will result in rejection of fabrics. With increasing use of patterned fabric, textile industry requires systems that produce more accurate defect detection. This research in answer to this demand proposed and enhanced techniques for patterned fabric defect detection. This techniques detects defect in two steps, namely, preprocessing and defect detection. The proposed defect detection systems are grouped as image data fusion based non-motif based method, wavelet based non-motif method and motif-based method. Several experiments were performed, all of which had the common goal of analyzing the applicability of the proposed algorithms for defect detection in patterned fabric images. These experiments were planned with the following two objectives.

1. To evaluate the performance of the preprocessing algorithm and to study its effect on defect detection

2. To evaluate the defect detection methods on their ability to identify defects in patterned fabrics

The results obtained are discussed in this chapter.

7.1. EXPERIMENTAL SETUP

Details regarding fabric dataset and performance metrics used during evaluation are presented in this section.

7.1.1. Dataset

In order to study the performance of the proposed algorithms, fabric images belonging to three major wallpaper groups (pmm, p2 and p4m groups whose lattices are of rectangular, parallelogram and Square shapes, respectively) are used. The reason behind selecting only these three groups is that all other wallpaper groups can be transformed into these three groups through geometric transformation (Ngan *et al.*, 2010a).

According to Hong Kong Productivity Council (2000), there are more than 90 types of defects that can degrade patterned fabrics. Out of this, this study considers five types of defects, namely, broken end, hole, netting multiple, thick bar and thin bar. Broken end is yarn breaking, running out or being prematurely released during insertion. Holes are the breakdown in the fabric where two or more adjacent yarns are severed to create an aperture for each hole. Netting multiple (double pick) is the insertion of two or several yarns in the same shed. Thin bar (dirty yarn) are yarns discolored by oil and thick bar (oil stain) is a discrete area of oil discoloration on a fabric. Example of the selected defects is presented in Figure 7.1.

The fabric image database used during experimentation consists of images 256 x 256 gray scale images belonging to wallpaper groups and other kinds of textures. The wallpaper group images were collected Wikipedia (http://en.wikipedia.org/wiki/Wallpaper_group). Other kind of textures images are subset of images obtained from TILDA dataset (http://lmb.informatik.uni-freiburg.de/research/dfg-texture/tilda). The TILDA dataset consists of 3200 real world textile images of 768 × 512 pixels gray scale images. To standardize the dataset, the Wikipedia images were first converted to gray scale at resolution 200 dpi and TILDA dataset was resized to 256 x 256 pixels. The images from Wikipedia were also used by Ngan *et al.* (2003, 2005). A template database was constructed by extracting lattices from all the images. A total of 600 images, out of which, 550 images are defect-free and 150 images had defects belonging to the five selected defect groups. Sample images under each of the 17

wallpaper groups (before conversion to grayscale) from the dataset are shown in Figure 7.2.

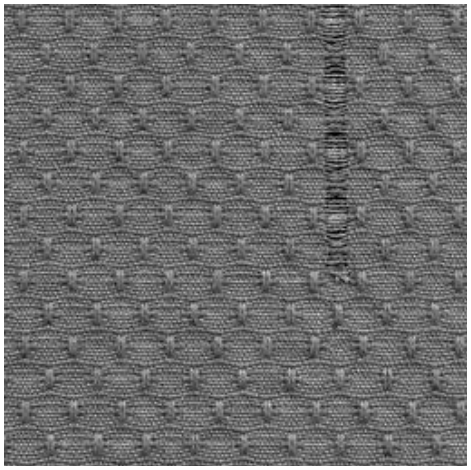

Broken End

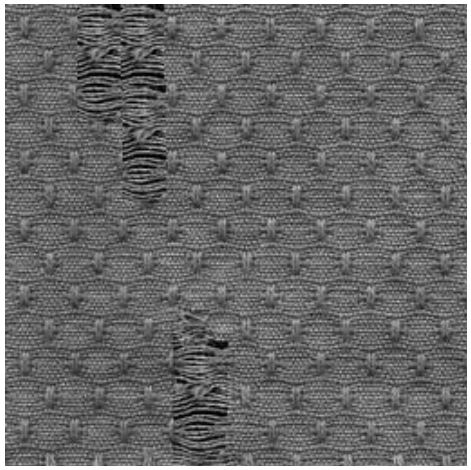

Holes

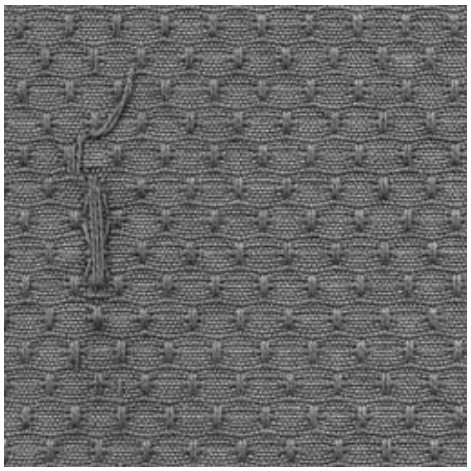

Netting Multiple

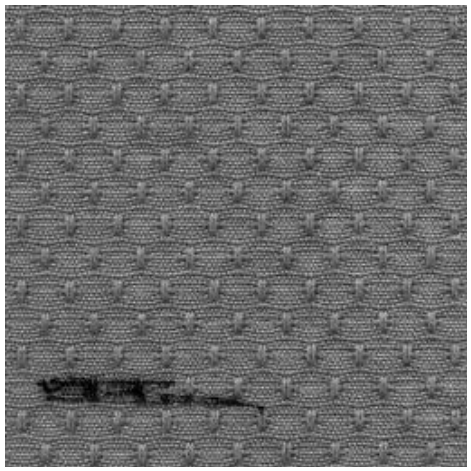

Thin Bar

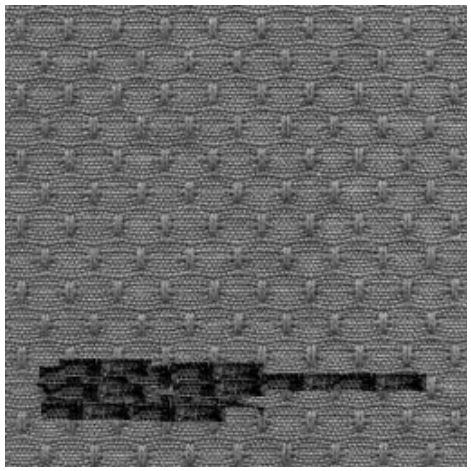

Thick Bar

Figure 7.1 : Examples of Selected Defects

p1

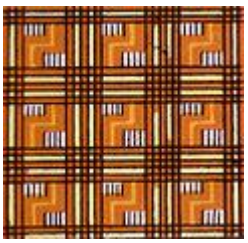

p2

pm

pg

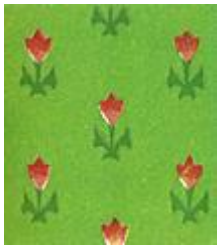

cm

pmm

pmg

pgg

cmm

p4

p4m

p4g

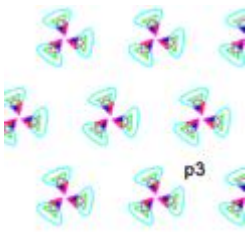

p3

p3m1

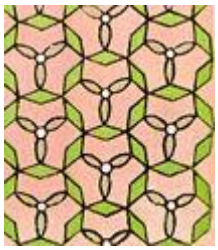

p31m

p6

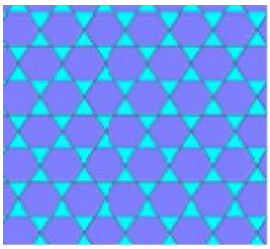

p6m

Figure 7.2 : Sample Images under Each Wallpaper Group

7.1.2. Performance Metrics

Different performance metrics were used to analyze the performance of Phase I and Phase II, III techniques. They are discussed in this section.

A) Preprocessing

To evaluate the proposed methods, four performance metrics were used. They analyze the algorithm's effectiveness in terms of image quality (Peak Signal to Noise Ratio), edge preservation capacity (Figure of Merit), structure preservation capacity (Mean Structural Similarity Index) and time complexity (Speed of enhancement). The method to calculate these metrics are presented below.

- **Peak Signal to Noise Ratio (PSNR)**

PSNR is an engineering term for the ratio between the maximum possible power of a signal and the power of corrupting noise that affects the fidelity of its representation. Because many signals have a very wide dynamic range, PSNR is usually expressed in terms of the logarithmic decibel scale. The PSNR is most commonly used as a measure of quality of reconstruction images. The higher the PSNR is the better the quality of the compressed or reconstructed image. To compute the PSNR, the block first calculates the mean-squared error using the following Equation (7.1).

$$MSE = \frac{\sum_{M,N}[I_1(m,n) - I_2(m,n)]^2}{M * N} \tag{7.1}$$

In the above equation, M and N are the number of rows and columns in the input images, respectively. Then the block computes the PSNR for gray scale images using the following Equation (7.2).

$$PSNR = 10 \log_{10}\left[\frac{R^2}{MSE}\right] \tag{7.2}$$

- **Edge Preservation Capacity**

The edge preservation capacity of the proposed algorithm is estimated using Pratt's Figure of Merit (FoM) (Yu and Acton, 2002) and is estimated using Equation (7.3).

$$FoM = \frac{1}{\max\{\hat{N}, N_{ideal}\}} \sum_{i=1}^{\hat{N}} \frac{1}{1 + d_i^2 \alpha} \tag{7.3}$$

where $\hat{N}$ and N_{ideal} are the number of detected and ideal edge pixels, respectively, d_i is the Euclidean distance between the i^{th} detected edge pixel and the nearest ideal edge pixel, and α is a constant typically set to 1/9. FOM ranges between 0 and 1, with unity for ideal edge detection.

- **Structure Preservation Capacity**

The structure preservation capacity of the preprocessing algorithm proposed is analyzed using Mean Structural Similarity Index (MSSI). The Mean Structural Similarity Index is a quality measure that is used to evaluate the overall image quality between the original (X) and the enhanced image (Y). Equation (7.4) is used to calculate this measure.

$$MSSI(x, y) = \frac{1}{M} \sum_{j=1}^{M} \frac{(2«_x «_y + c_1)(2cov_{xy} + c_2)}{(«_x^2 + «_y^2 + c_1)(±_x^2 + ±_y^2 + c_2)} \tag{7.4}$$

where M is the number of local windows, μ_x is the average of x, μ_y is the average of y, σ_x^2 is the variance of x, σ_y^2 is the variance of y, and cov_{xy} the covariance of x and y. c_1 and c_2 are two small values included to stabilize the division with weak denominator (Wang *et al.*, 2004). In this research, 8 x 8 window size is used during experimentation.

- **Time Complexity**

Denoising time is the execution taken by the filters to perform the operation of impulse noise removal on the noisy image and obtain the reconstructed image. The time is measured in seconds. Enhancement speed depends on the following characteristics.

- The complexity of the algorithm
- The efficiency of the implementation of the algorithm
- The speed of the processor hardware

Generally, the desired behavior is to have increased speed during recognition process.

B) Defect Detection

To evaluate the performance of non-motif and motif-based defect detection algorithms, four parameters namely, sensitivity, specificity, detection success rate (accuracy) and speed are used.

Sensitivity is defined as proportion of actual positives which are predicted positive (Equation 7.5). In other terms, it is the correct detection of defective samples.

$$\text{Sensitivity}=TP / (TP + FN) \quad (7.5)$$

Specificity is defined as the proportion of actual negative which are negative (Equation 7.6). In other words, it is correct detection of defect free samples.

$$\text{Specificity}=TN / (TN + FP) \quad (7.6)$$

Accuracy is the ratio of number of samples correctly prediction to the total number of samples (Equation 7.7).

$$\text{Accuracy} = (TP + TN) / (TP + TN + FP + FN) \quad (7.7)$$

The definitions TP (True Positive), TN (True Negative), FP (False Positive) and FN (False Negative) is according to Table 7.1, which presents the confusion matrix.

TABLE 7.1

DEFINITION OF TP, TN, FP AND FN

	Actually Defective	Actually Defect-Free
Detected as Defective	TP (True Positive)	FP (False Positive)
Detected as Defect-Free	FN (False Negative)	TN (True Negative)

7.2. EXPERIMENTAL RESULTS OF PREPROCESSING

To analyze the performance of the preprocessing algorithm in its efficiency to enhance an input image, the test images in Figure 7.3 were used. For evaluation, impulse noise was introduced artificially introduced and the corrupted images were obtained by varying noise density from 0.1 - 0.9% in steps of 0.1. In the tables and graphs, the existing denoising method is referred as KWF and the proposed denoising method is referred as EDSMF (Enhanced Directional Switching Median Filter).

Table 7.2 shows the performance of the existing and proposed algorithm with respect to image quality measured in terms of Peak Signal to Noise Ratio. Tables 7.3 and 7.4 present the FoM and MSSI values obtained for the selected test images. The time taken by the KWF and EDSMF methods to perform enhancement operations is given in Table 7.5.

(a) TPF1

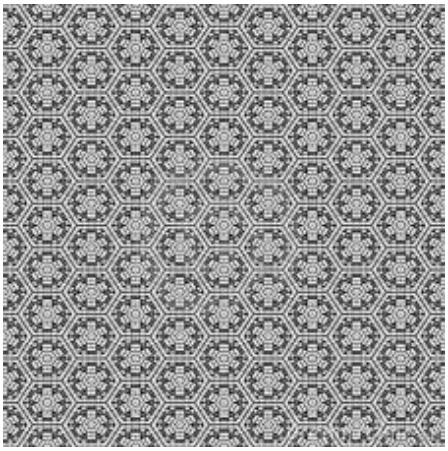

(b) TPF2

(c) TPF3

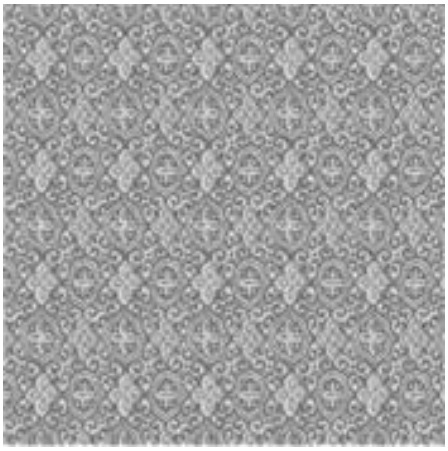

(d) TPF4

Figure 7.3 : Test Images

From the results, it is clear that proposed EDSMF method has improved the performance of the impulse noise filtering process in terms of PSNR, FoM, MSSI and execution speed. It can further be seen that increase in impulse noise, as expected, decreases the quality of denoised image. Even with the highest noise density (0.9%), the PSNR of the proposed system was on average 40.58dB, which was 38.4dB for the EWF method. With the lowest noise density, on average the PSNR obtained while using the proposed method was 28.23dB as opposed to 25.71db obtained by the existing method. Overall, on average, the proposed method showed 6.02% quality gain when compared with base KWF method.

TABLE 7.2

PEAK SIGNAL TO NOISE RATIO (dB)

Noise Density	TPF1		TPF2		TPF3		TPF4	
	KWF	EDSMF	KWF	EDSMF	KWF	EDSMF	KWF	EDSMF
0.1	39.17	41.85	38.13	40.29	38.01	39.21	38.28	40.96
0.2	37.95	40.37	37.00	38.97	36.79	38.46	37.06	39.48
0.3	36.87	38.18	35.71	37.29	35.47	37.02	35.98	37.48
0.4	34.87	36.65	33.71	35.26	33.14	35.11	33.68	35.75
0.5	33.56	35.71	32.40	34.12	32.11	33.55	32.67	34.82
0.6	31.37	33.89	30.21	33.00	29.92	32.73	30.48	32.41
0.7	30.12	31.77	28.99	31.14	28.54	30.97	29.23	31.33
0.8	27.46	30.55	27.09	29.66	26.97	29.08	27.22	29.94
0.9	26.54	28.77	25.38	28.00	25.27	27.89	25.65	28.26

TABLE 7.3

EDGE PRESERVATION CAPACITY (FoM)

Noise Density	TPF1		TPF2		TPF3		TPF4	
	KWF	EDSMF	KWF	EDSMF	KWF	EDSMF	KWF	EDSMF
0.1	0.8110	0.8153	0.8034	0.8040	0.7982	0.8018	0.8039	0.8127
0.2	0.7832	0.7925	0.7740	0.7763	0.7779	0.7867	0.7816	0.7828
0.3	0.7398	0.7468	0.7301	0.7341	0.7240	0.7301	0.7356	0.7403
0.4	0.7203	0.7320	0.7088	0.7197	0.6968	0.7025	0.7166	0.7238
0.5	0.7027	0.7325	0.6978	0.6933	0.6874	0.6944	0.7018	0.7084
0.6	0.6433	0.7007	0.6272	0.6342	0.6197	0.6224	0.6359	0.6465
0.7	0.6317	0.6522	0.6235	0.6329	0.6127	0.6199	0.6243	0.6382
0.8	0.6202	0.6619	0.6144	0.6195	0.6079	0.6130	0.6183	0.6303
0.9	0.6148	0.6380	0.6046	0.6133	0.6065	0.5976	0.6123	0.6289

TABLE 7.4

STRUCTURE PRESERVATION CAPACITY (MSSI)

Noise Density	TPF1		TPF2		TPF3		TPF4	
	KWF	EDSMF	KWF	EDSMF	KWF	EDSMF	KWF	EDSMF
0.1	0.8310	0.8508	0.8318	0.8353	0.8320	0.8361	0.8303	0.8385
0.2	0.8037	0.8693	0.8371	0.8393	0.8344	0.8354	0.8305	0.8364
0.3	0.7921	0.8125	0.8359	0.8361	0.8314	0.8319	0.8362	0.8377
0.4	0.7787	0.7941	0.8340	0.8349	0.8323	0.8326	0.8318	0.8327
0.5	0.7757	0.7867	0.8322	0.8381	0.8343	0.8388	0.8356	0.8391
0.6	0.7236	0.7557	0.8338	0.8375	0.8317	0.8363	0.8308	0.8315
0.7	0.7006	0.7228	0.8313	0.8343	0.8320	0.8385	0.8369	0.8317
0.8	0.6856	0.7051	0.8331	0.8350	0.8321	0.8323	0.8339	0.8368
0.9	0.6409	0.6883	0.8310	0.8351	0.8370	0.8305	0.8323	0.8374

TABLE 7.5

SPEED OF PREPROCESSING (in SECONDS)

Noise Density	TPF1		TPF2		TPF3		TPF4	
	KWF	EDSMF	KWF	EDSMF	KWF	EDSMF	KWF	EDSMF
0.1	1.01	0.99	1.18	1.14	1.23	1.10	1.13	1.09
0.2	1.01	0.99	1.18	1.14	1.23	1.10	1.13	1.09
0.3	1.01	0.99	1.20	1.14	1.24	1.10	1.14	1.09
0.4	1.09	1.05	1.21	1.14	1.24	1.11	1.14	1.09
0.5	1.09	1.05	1.21	1.14	1.24	1.11	1.14	1.11
0.6	1.12	1.05	1.21	1.16	1.24	1.12	1.15	1.11
0.7	1.12	1.06	1.22	1.16	1.26	1.12	1.15	1.11
0.8	1.13	1.06	1.22	1.16	1.26	1.12	1.15	1.13
0.9	1.14	1.06	1.22	1.16	1.26	1.12	1.16	1.13

Pratt’s FoM is used to evaluate the edge preserving performance of the KWF and proposed methods with different noise density values. Again it could be seen that the EDSMF method has improved edge preservation which is evident by the nearing to unity values achieved. On average, the proposed method, showed an average efficiency gain of 1.24% when compared to the existing method with respect to FoM.

The MSSI values obtained reveal that the structure preserving capacity of the proposed method has improved when compared with the existing KWF method. This is ascertained by the near to unity MSSI values obtained by the EDSMF method.

From the tabulated results pertaining to speed, it could be seen that variation in noise density does not affect time taken to denoise. The speed ranged between the 1.01-1.26 seconds for KWF method while it was between 0.99 and 1.16 seconds for the proposed EDSMF method. Thus, the runtime analysis reveals that the EDSMF method produces better denoising results. On average, the KWF method took less than 1.17 seconds while it was 1.10 seconds for the proposed method, which showed a speed efficiency gain of 5.87%.

Figure 7.4 to 7.7 shows the visual comparison of the experimental results for two noise density, 0.2% and 0.9% of the four selected test images.

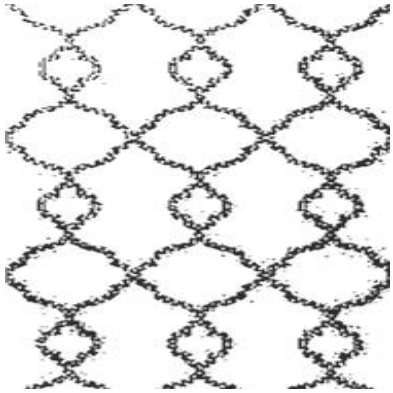

Original Image (after grayscale conversion)

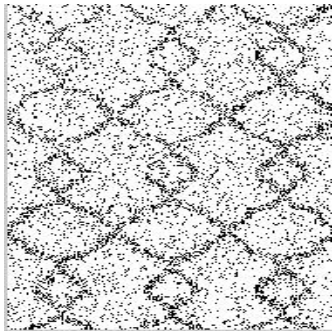

Noisy Image (0.2%)

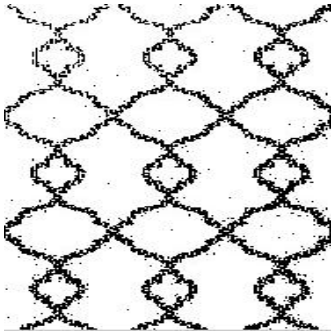

Enhanced Image (KMF)

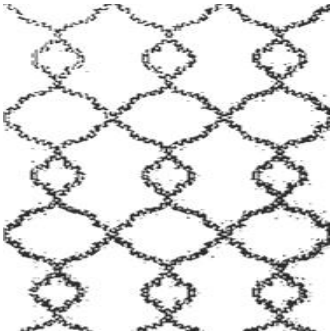

Enhanced Image (EDSMF)

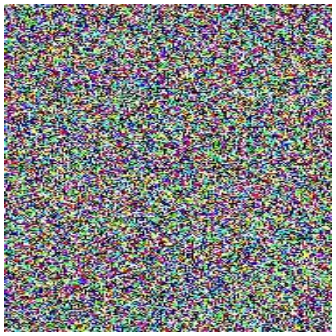

Noisy Image (0.9%)

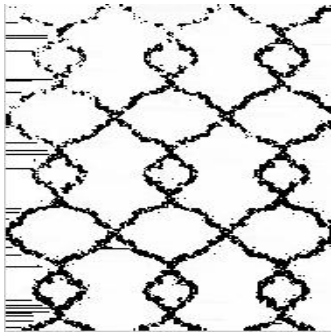

Enhanced Image (KMF)

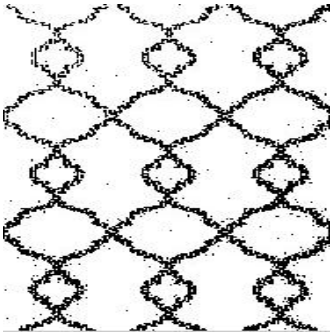

Enhanced Image (EDSMF)

Figure 7.4 : Visual Results of TPF1 Image

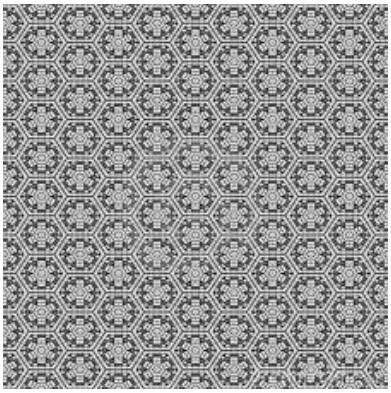

Original Image (after grayscale conversion)

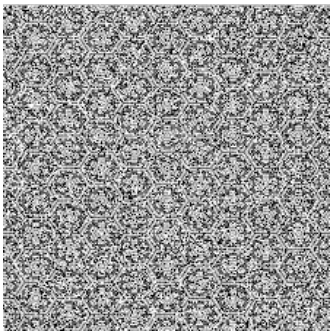

Noisy Image (0.2%)

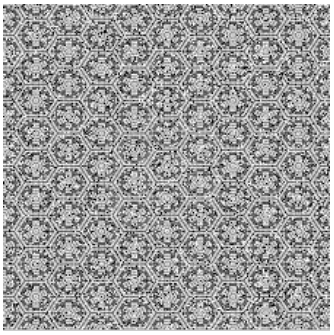

Enhanced Image (KWF)

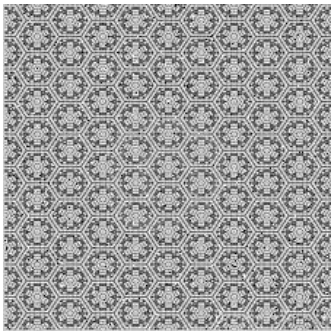

Enhanced Image (EDSMF)

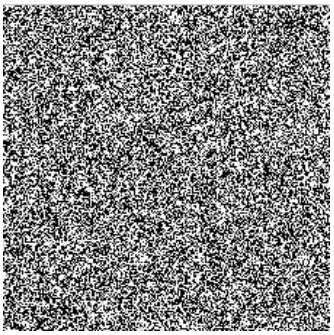

Noisy Image(0.9%)

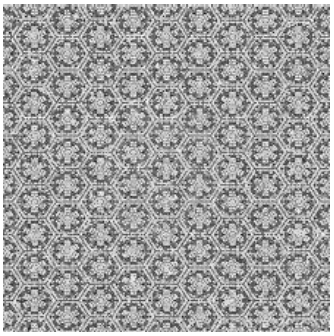

Enhanced Image (KWF)

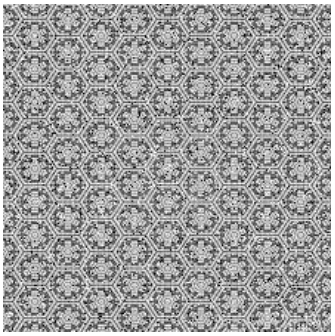

Enhanced Image (EDSMF)

Figure 7.5 : Visual Results of TPF2 Image

Original Image (after grayscale conversion)

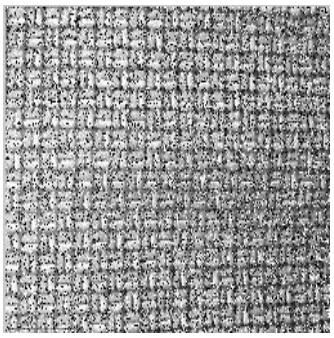

Noisy Image (0.2%)

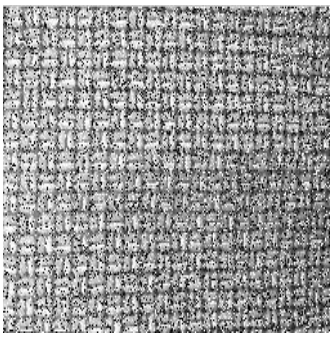

Enhanced Image (KWF)

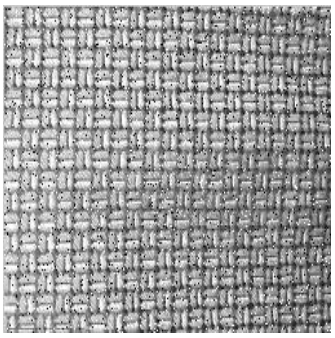

Enhanced Image (EDSMF)

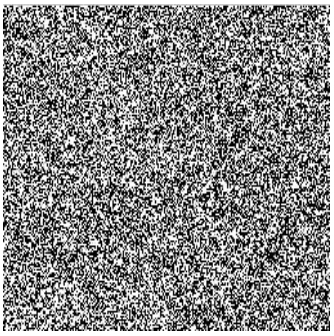

Noisy Image(0.9%)

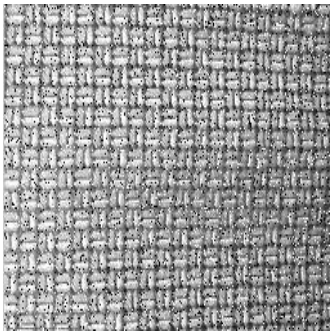

Enhanced Image (KWF)

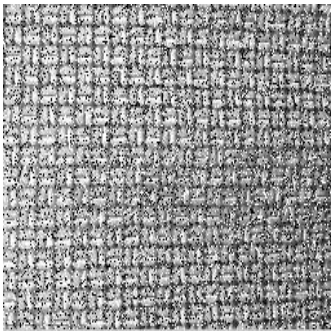

Enhanced Image (EDSMF)

Figure 7.6 : Visual Results of TPF3 Image

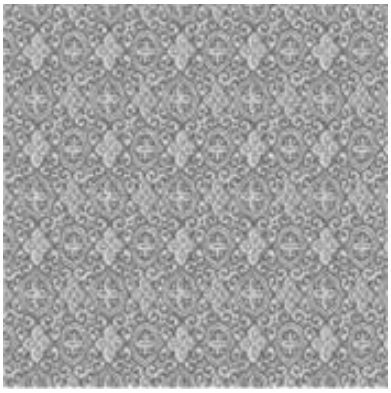

Original Image (after grayscale conversion)

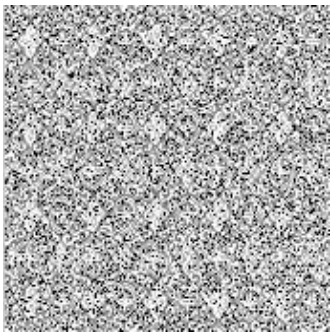

Noisy Image (0.2%)

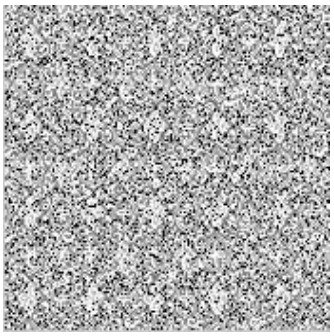

Enhanced Image (KWF)

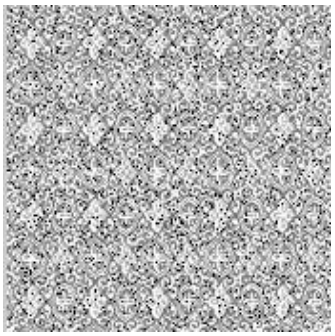

Enhanced Image (EDSMF)

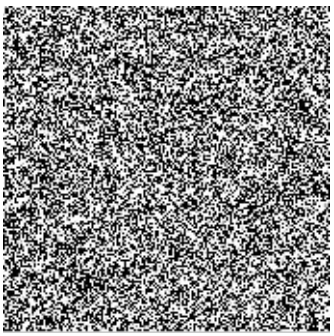

Noisy Image(0.9%)

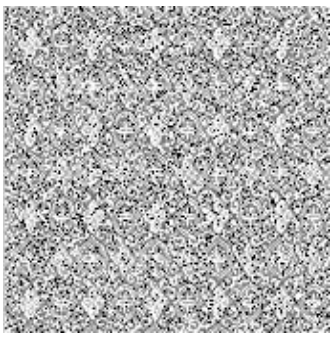

Enhanced Image (KWF)

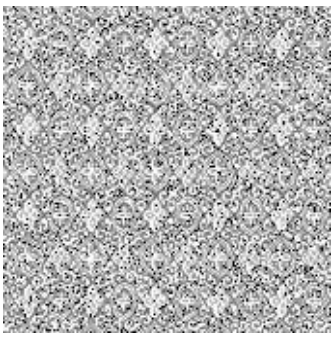

Enhanced Image (EDSMF)

Figure 7.7 : Visual Results of TPF4 Image

7.3. EXPERIMENTAL RESULTS OF FABRIC DEFECT DETECTION

The present research work proposes 14 enhanced defect detection models, out of which, 13 are non-motif-based and one is motif based. The models allotted codes for ease of discussion and the coding scheme used is given in Table 7.6. The rest of this section presents the results obtained by the proposed and existing detection methods in terms of sensitivity, specificity, accuracy and speed.

7.3.1. Experimental Results of Non-Motif-Based Models

Tables 7.7 and 7.8 show the sensitivity of the proposed 13 non-motif-based models (1 fusion and 13 wavelet based). The results are compared with existing model (WGIS). The results are presented for the five selected defects, namely, broken end, hole, netting multiple, thick bar and thin bar. To ascertain the overall performance of the non-motif based systems, the average sensitivity and specificity of all the five defects were calculated and the results are presented in Figures 7.9 and 7.10 respectively.

From the results of sensitivity, it can be seen that among the non-motif based models, all the proposed models improves the defect detection when compared with the existing model. Comparison between fusion based and enhanced wavelet based models, the enhanced wavelet based models show better performance. Comparison between the two types of wavelets, optimal wavelet tree and Gabor wavelets, the Gabor wavelet based models showed better results. Among the three selection algorithms, VQ + PCA, ICA and VQ + PCA + ICA algorithm, the algorithm performing multiple projections using VQ+PCA and ICA portrayed more sensitivity. All the models were efficient in detecting broken defects, followed by hole, netting multiple, oil stains and dirty defects in fabrics. The GVPIN model showed the maximum average sensitivity of 89.33%. A maximum sensitiveness of 93.08% was achieved by the same model for detecting broken defects.

TABLE 7.6

CODING SCHEME USED

	Description	Code
1	Wavelet and GIS Algorithm	WGIS
2	Image Data Fusion	IDF
3	Optimal Wavelet Tree based GIS Algorithm using VQ + PCA Projections	OGVP
4	Optimal Wavelet Tree based GIS Algorithm using ICA Projections	OGI
5	Optimal Wavelet Tree based GIS Algorithm using VQ + PCA + ICA Projections	OGVPI
6	Optimal Wavelet Tree using VQ + PCA Projections on Neural Network	OVPN
7	Optimal Wavelet Tree based using ICA Projections on Neural Network	OIN
8	Optimal Wavelet Tree based using VQ + PCA + ICA Projections on Neural Network	OVPIN
9	Gabor Wavelets based GIS Algorithm using VQ + PCA Projections	GGVP
10	Gabor Wavelets based GIS Algorithm using ICA Projections	GGI
11	Gabor Wavelets based GIS Algorithm using VQ + PCA + ICA Projections	GGVPI
12	Gabor Wavelets using VQ + PCA Projections on Neural Network	GVPN
13	Gabor Wavelets based using ICA Projections on Neural Network	GIN
14	Gabor Wavelets based using VQ + PCA + ICA Projections on Neural Network	GVPIN
15	Motif-based Defect Detection System	MBM
16	Enhanced Motif-based Defect Detection System with Autocorrelation and Spatial Information	EMBMAS

TABLE 7.7

SENSITIVITY (%) OF THE NON-MOTIF-BASED MODELS

Models	Broken	Hole	Netting Multiple	Thick Bar	Thin Bar
WGIS	82.96	82.50	80.18	80.48	79.83
IDF	85.68	84.44	81.95	81.67	80.69
OGVP	86.41	84.34	82.77	82.28	81.29
OGI	86.12	84.73	82.90	82.11	81.58
OGVPI	87.43	84.71	83.02	82.20	81.95
OVPN	88.56	86.33	84.56	82.95	82.90
OIN	87.97	85.34	84.37	82.27	82.59
OVPIN	88.98	86.13	85.17	84.05	83.59
GGVP	91.21	86.93	86.11	84.48	85.19
GGI	90.33	86.68	86.37	83.94	85.06
GGVPI	90.62	88.66	86.24	84.51	85.37
GVPN	92.33	90.37	87.98	86.01	87.17
GIN	92.65	89.30	87.39	85.96	86.90
GVPIN	93.08	90.58	88.28	87.52	87.21

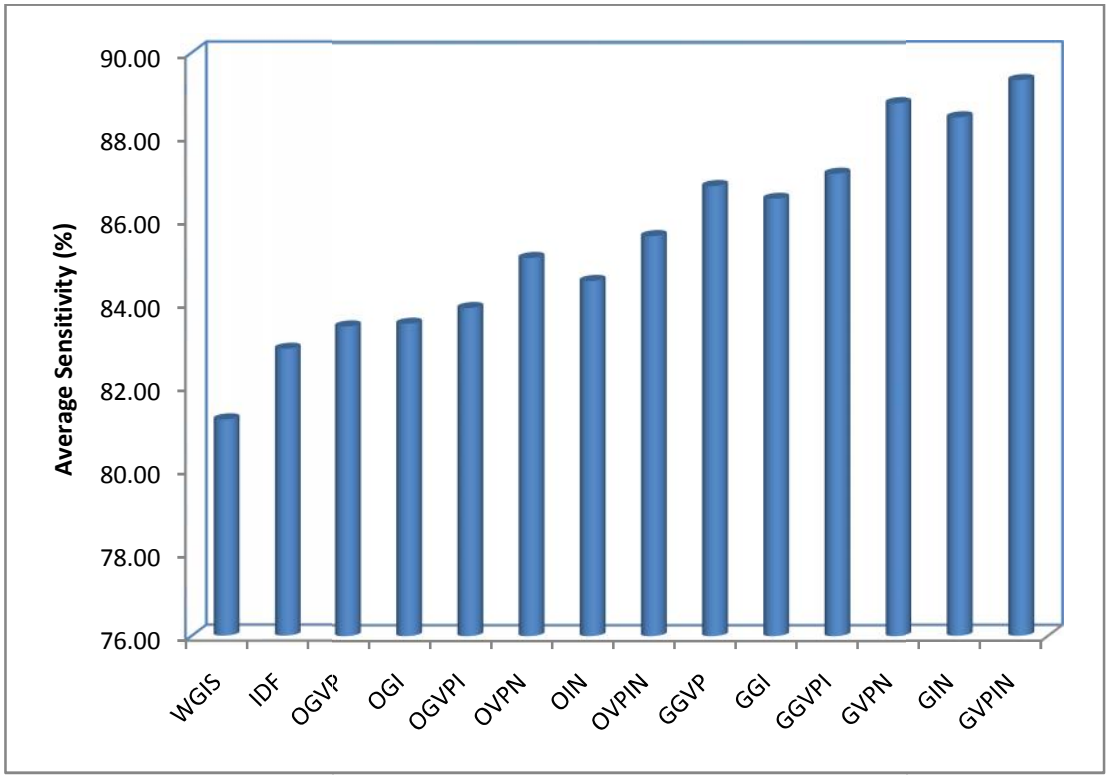

Figure 7.8 : Average Sensitivity (%)

TABLE 7.8

SPECIFICITY (%) OF THE NON-MOTIF-BASED MODELS

Models	Broken	Hole	Netting Multiple	Thick Bar	Thin Bar
WGIS	84.82	83.41	83.35	82.83	83.91
IDF	85.62	85.06	85.58	84.97	85.26
OGVP	86.79	85.61	85.24	85.09	86.10
OGI	85.95	85.35	85.11	84.97	85.83
OGVPI	86.83	85.85	86.35	85.23	85.60
OVPN	88.06	86.97	86.69	85.86	86.44
OIN	87.10	86.98	86.40	85.22	86.30
OVPIN	88.24	87.19	88.24	86.96	87.30
GGVP	89.62	88.86	89.28	88.78	88.69
GGI	89.88	88.11	88.37	88.44	88.85
GGVPI	90.82	89.32	88.76	88.83	89.32
GVPN	92.59	91.63	90.61	89.92	90.50
GIN	92.54	91.53	90.54	89.63	90.17
GVPIN	93.88	92.25	91.44	90.31	90.47

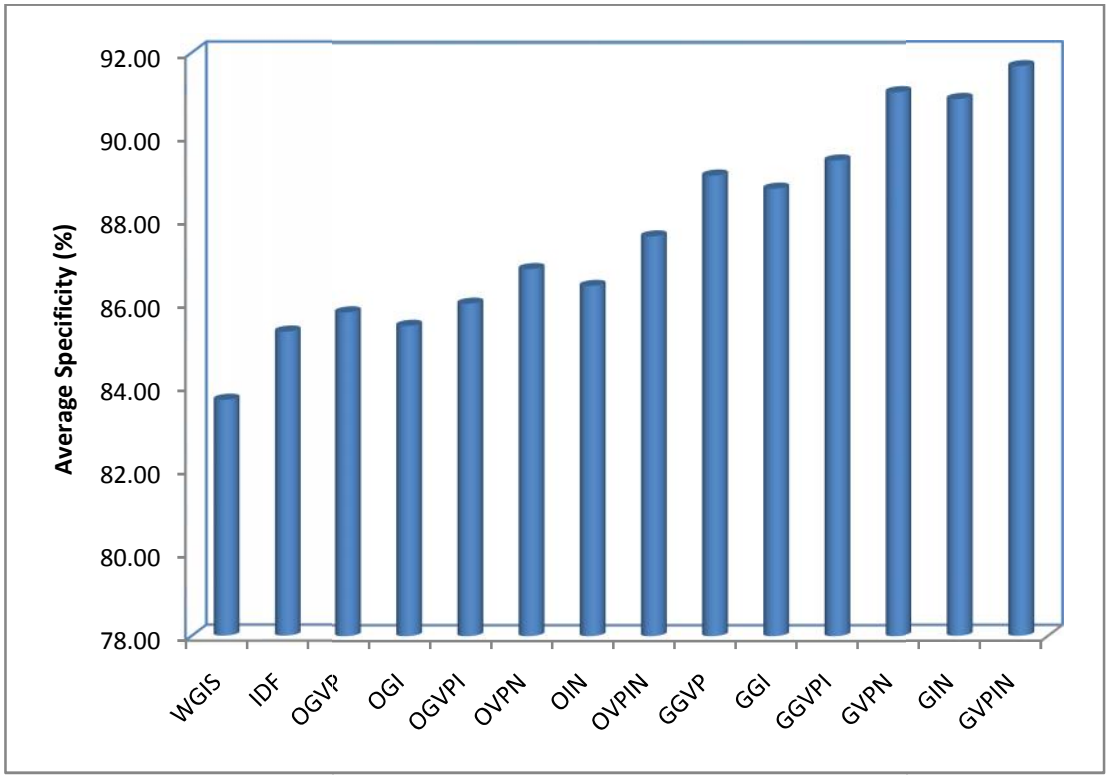

Figure 7.9 : Average Specificity (%)

From Table 7.8 and Figure 7.10, it is evident that the trend obtained with sensitivity and specificity is similar. The GVPIN model showed the maximum average specificity of 91.67%. A maximum specificity of 93.88% was achieved by the same model for detecting broken defects, followed by 92.25 with detecting hole defect in patterned fabrics. The GVPIN model, thus on average, shows an average efficiency of 8.74% when compared to the existing model WGIS model.

The accuracy of defect detection produced by the various proposed models and existing models of Phase II is given in Table 7.9. Figure 7.11 shows the average accuracy to compare the overall performance of the models.

The defect detection accuracy results also show that while all the proposed models produce high accuracy when compared to the existing model, the wavelet based model produce better results than fusion based defect detection model. Maximum accuracy was produced while using Gabor wavelets combined with multiple projection-based selection algorithm, namely, VQ + PCA + ICA. The algorithms produced high detection accuracy when presented with fabrics having broken defects, followed by hole and netting multiple defects. Thick and thin fabric defects, eventhough produced high results, were still low when compared with other defects.

The GVPIN model showed an average accuracy of 91.99%. A maximum sensitiveness of 94.88% was achieved by the same model for detecting broken defects. Following this, the GVPIN model produced an average accuracy of 91.55% and 94.33% for detecting broken defects. Lowest performance was shown by the fusion based model (88.36%). The existing model, WGIS, showed an average detection accuracy of 82.62% and 86.61% with broken defects. From the average results, a 10.19% efficiency gain with respect to accuracy was achieved by GVPIN when compared with WGIS model.

Table 7.10 shows the speed of defect detection by the various algorithms presented in Phase II of the study. The results are compared again with the existing model, WGIS. To analyze the overall speed efficiency, the average time was calculated and the result is presented in Figure 7.11.

TABLE 7.9

ACCURACY (%) OF THE NON-MOTIF-BASED MODELS

Models	Broken	Hole	Netting Multiple	Thick Bar	Thin Bar
WGIS	86.61	83.35	81.87	79.97	81.30
IDF	88.36	84.91	83.69	81.10	82.47
OGVP	88.93	86.40	85.36	82.42	84.43
OGI	88.70	85.80	84.43	82.08	83.46
OGVPI	89.61	87.11	86.14	83.30	84.85
OVPN	90.42	88.41	87.03	84.38	85.70
OIN	89.85	87.96	86.66	83.97	85.12
OVPIN	91.05	88.97	87.16	85.18	86.12
GGVP	92.92	90.59	88.78	86.66	87.81
GGI	92.36	90.23	88.54	86.37	87.42
GGVPI	92.97	91.55	89.28	87.01	88.53
GVPN	94.33	93.10	91.27	88.90	90.15
GIN	93.89	92.86	90.77	88.53	89.72
GVPIN	94.88	93.18	91.50	89.54	90.85

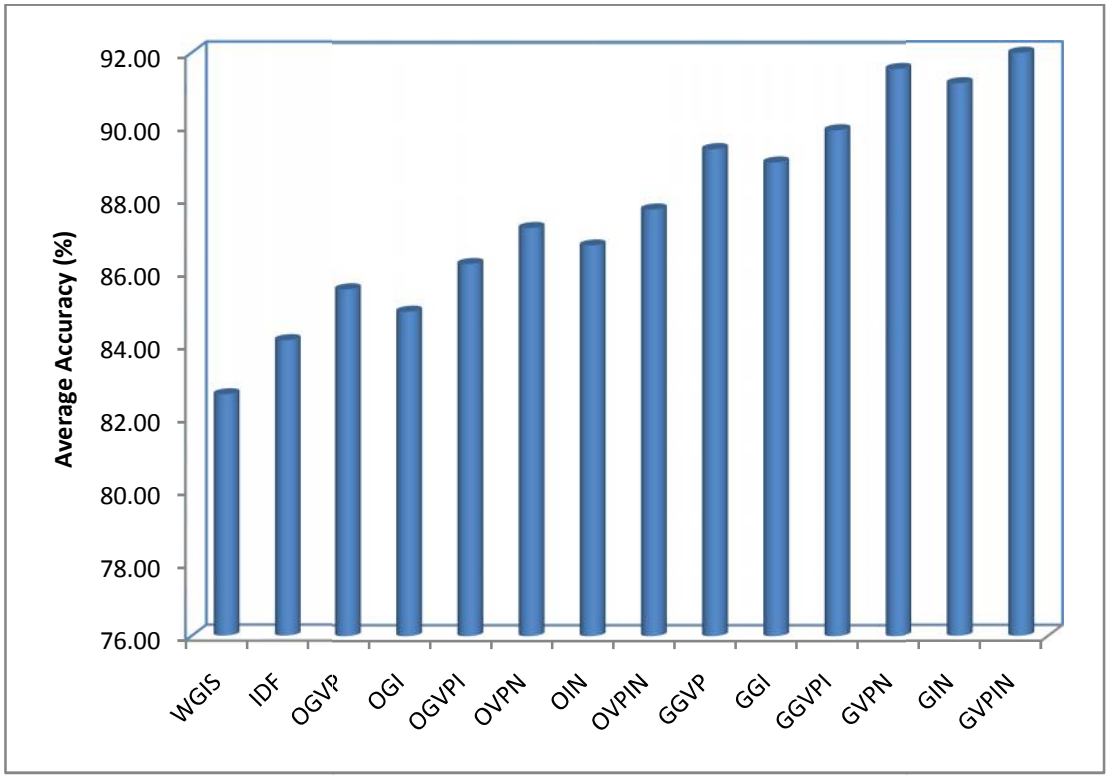

Figure 7.10 : Average Accuracy (%)

TABLE 7.10

SPEED (in SECONDS) OF THE NON-MOTIF-BASED MODELS

Models	Broken	Hole	Netting Multiple	Thick Bar	Thin Bar
WGIS	0.58	0.58	0.58	0.59	0.59
IDF	0.31	0.31	0.31	0.31	0.30
OGVP	0.44	0.43	0.43	0.44	0.44
OGI	0.45	0.46	0.47	0.46	0.45
OGVPI	0.42	0.42	0.42	0.43	0.41
OVPN	0.38	0.39	0.38	0.38	0.38
OIN	0.39	0.39	0.39	0.38	0.40
OVPIN	0.36	0.36	0.37	0.36	0.36
GGVP	0.54	0.54	0.56	0.55	0.44
GGI	0.56	0.56	0.57	0.56	0.45
GGVPI	0.53	0.53	0.54	0.53	0.41
GVPN	0.50	0.51	0.51	0.50	0.38
GIN	0.52	0.52	0.53	0.52	0.40
GVPIN	0.46	0.47	0.46	0.47	0.36

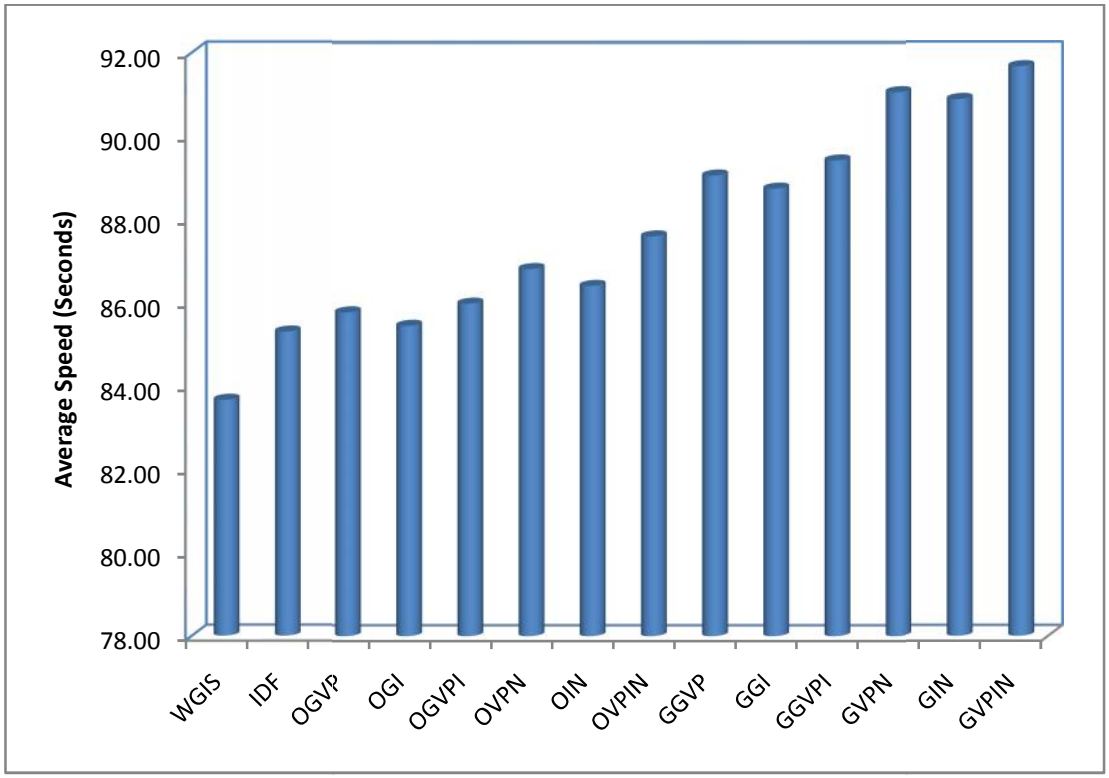

Figure 7.11 : Average Speed (in Seconds)

The results with respect to speed show a different trend than the one obtained with the other performance metrics, namely, sensitivity, specificity and accuracy. With respect to time taken to detect defects in patterned fabrics, the fusion based algorithm was the fastest when compared with other models. The average speed obtained by IDF model is 0.31 seconds. The speed efficiency obtained while using the multiple projection based selection algorithm (VA + PCA + ICA) shows that the selection algorithm is effective in reducing the number of coefficients and thus, the computation complexities. The results further show that the type of defect does not have any impact on the speed of defect detection.

7.3.2. Experimental Results of Motif-Based Models

Table 7.11 shows the sensitivity, specificity, accuracy and speed of the existing and proposed motif-based models.

TABLE 7.11

PERFORMANCE OF MOTIF-BASED MODELS

Metric	Model	Broken	Hole	Netting Multiple	Thick Bar	Thin Bar
Sensitivity (%)	EMBMAS	95.92	93.52	92.07	90.47	89.72
	MBM	93.20	91.80	89.39	89.00	89.03
Specificity (%)	EMBMAS	96.09	95.15	93.75	92.19	92.51
	MBM	95.17	93.40	92.97	91.61	90.96
Accuracy (%)	EMBMAS	98.23	96.23	94.56	92.57	92.31
	MBM	96.72	94.62	93.15	91.15	91.97
Speed (Seconds)	EMBMAS	0.33	0.33	0.32	0.34	0.32
	MBM	0.34	0.34	0.34	0.35	0.34

Results from all the four parameters show that the enhanced motif based model is efficient in detecting defects. The proposed algorithm is efficient with

broken defects, followed by holes. A maximum accuracy of 98.23% was achieved with broken defected patterned fabric. Figures 7.12 a-d present the average results of the proposed and existing motif-based models for the four selected performance metrics.

On average, the proposed EMBMAS model showed an efficiency gain of 2.01% in terms of sensitivity, 1.19% in terms of specificity and 1.33% in terms of accuracy, when compared with the existing MBM model. On average, the EMBMAS algorithm showed a minimum speed difference of 0.01 seconds over MBM algorithm. These positive results show that the autocorrelation method for automatic lattice and motif extraction and inclusion of spatial relationship is advantageous when applied to detect defects on wallpaper groups of patterned fabrics.

Table 7.10 shows the overall comparison of the best models from both motif and non-motif based models. The results are again compared with the existing counterparts.

This comparison stresses the fact that the proposed models (both motif and non-motif) works better than existing models with respect to all performance measures. Comparison between motif and non-motif models reveals motif-based models as a better algorithm for patterned fabric defect detection.

Figures 7.13 to 7.17 presents the visual result of the two patterned fabric defect detection models, GVPIN and EMBMAS models for the five defects broken end , hole, netting multiple, thick bar and thin bar respectively and the results are compared with the existing counterparts WGIS and MBM models.

This chapter presented the results of the experiments conducted to evaluate the various proposed models in Phases I, II and III of the study. The work is summarized and concluded in the next chapter, Summary and Conclusion.

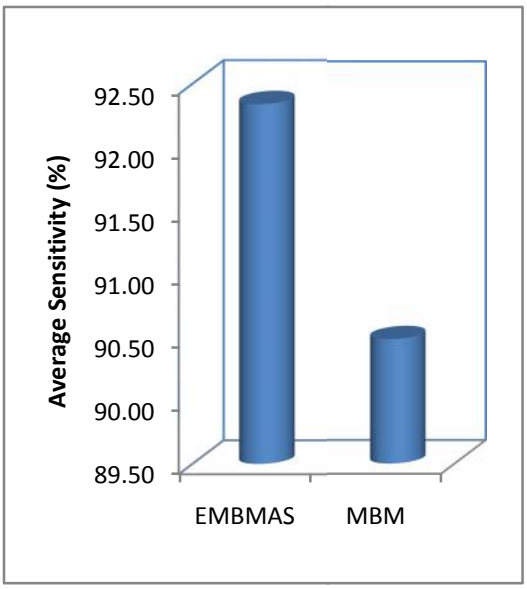

(a) Average Sensitivity (%)

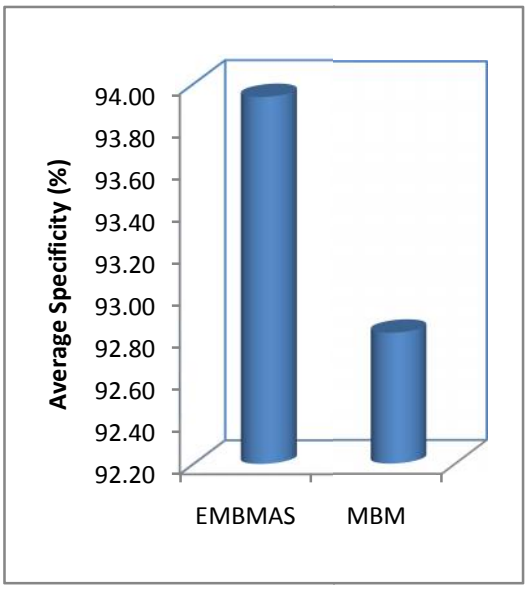

(b) Average Specificity (%)

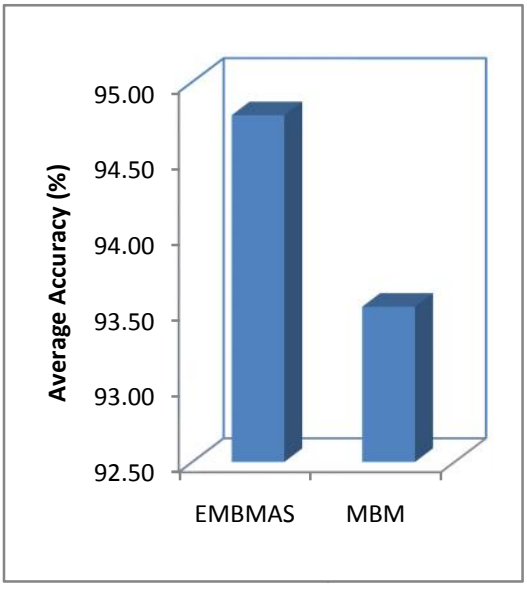

(c) Average Accuracy (%)

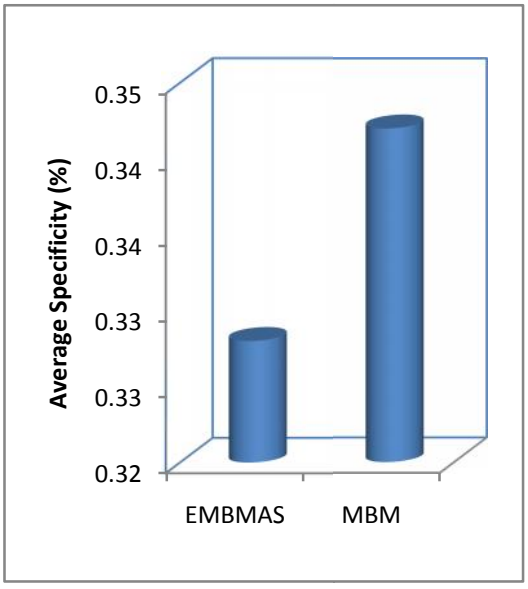

(d) Average Speed (Seconds)

Figure 7.12 : Average Performance of Motif-Based Models

TABLE 7.12

OVERALL COMPARISON

Metric	Model	Broken	Hole	Netting Multiple	Thick Bar	Thin Bar
Sensitivity (%)	WGIS	82.96	82.50	80.18	80.48	79.83
	GVPIN	93.08	90.58	88.28	87.52	87.21
	MBM	93.20	91.80	89.39	89.00	89.03
	EMBMAS	95.92	93.52	92.07	90.47	89.72
Specificity (%)	WGIS	84.82	83.41	83.35	82.83	83.91
	GVPIN	93.88	92.25	91.44	90.31	90.47
	MBM	95.17	93.40	92.97	91.61	90.96
	EMBMAS	96.09	95.15	93.75	92.19	92.51
Accuracy (%)	WGIS	86.61	83.35	81.87	79.97	81.30
	GVPIN	94.88	93.18	91.50	89.54	90.85
	MBM	96.72	94.62	93.15	91.15	91.97
	EMBMAS	98.23	96.23	94.56	92.57	92.31
Speed (Seconds)	WGIS	0.58	0.58	0.58	0.59	0.59
	GVPIN	0.46	0.47	0.46	0.47	0.36
	MBM	0.34	0.34	0.34	0.35	0.34
	EMBMAS	0.33	0.33	0.32	0.34	0.32

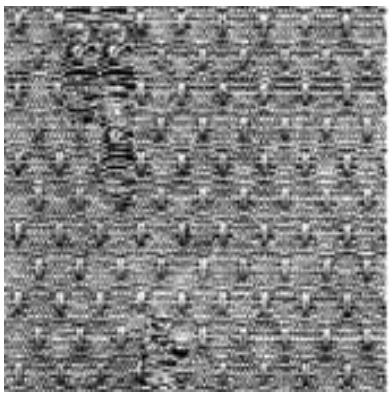

(a) Original

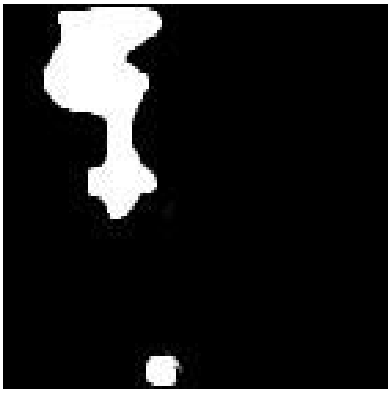

(b) WGIS Model

(c) GVPIN Model

(d) MBM Model

(e) EMBMAS Model

Figure 7.13 : Visual Results of Broken End Defect Detection

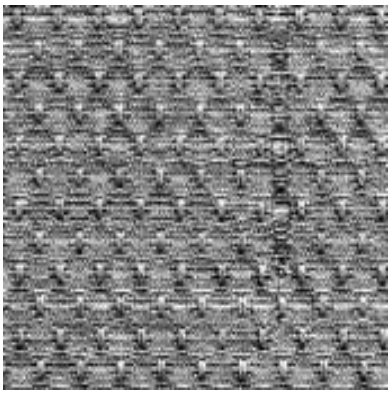

(a) Original

(b) WGIS Model

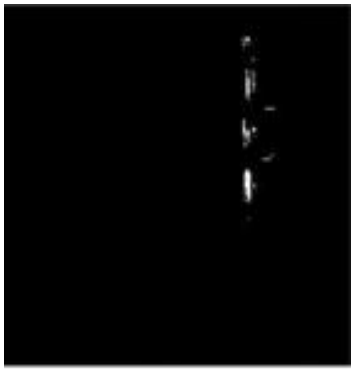

(c) GVPIN Model

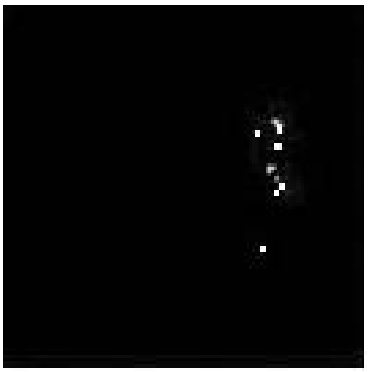

(d) MBM Model

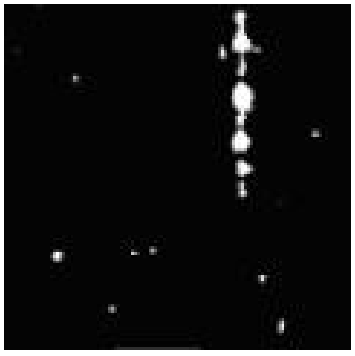

(e) EMBMAS Model

Figure 7.14 : Visual Results of Holes Defect Detection

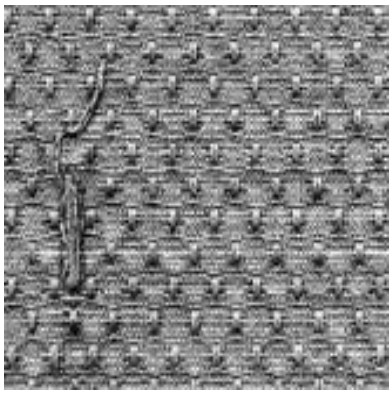

(a) Original

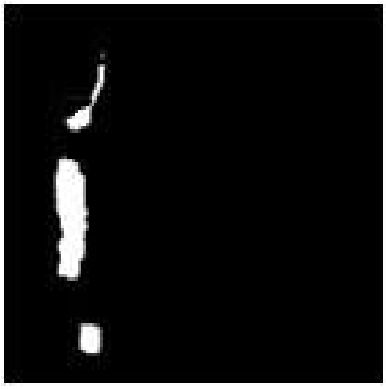

(b) WGIS Model

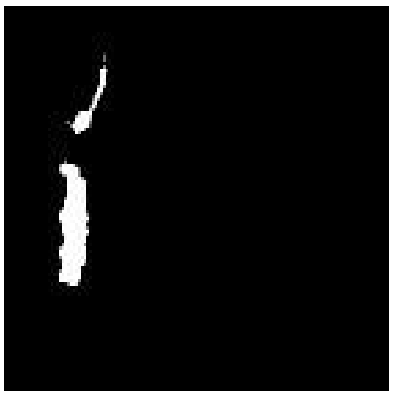

(c) GVPIN Model

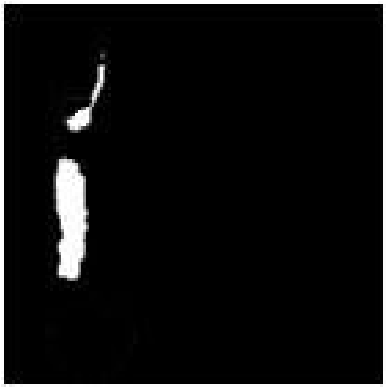

(d) MBM Model

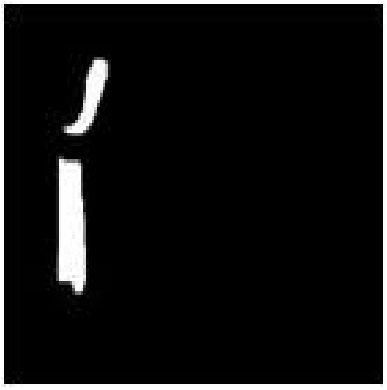

(e) EMBMAS Model

Figure 7.15 : Visual Results of Netting Multiples Defect Detection

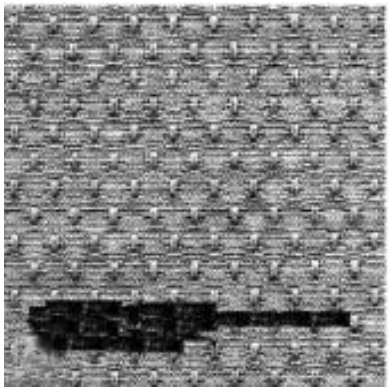

(a) Original

(b) WGIS Model

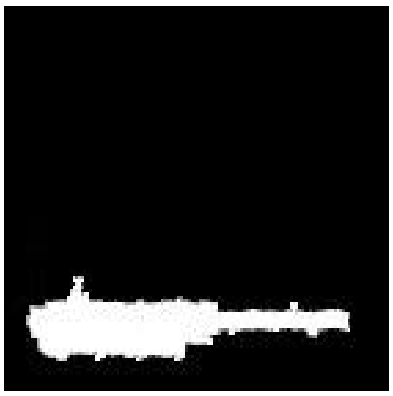

(c) GVPIN Model

(d) MBM Model

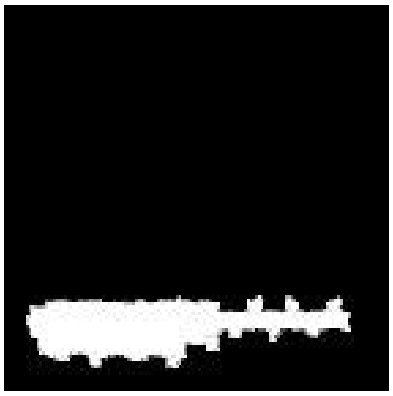

(e) EMBMAS Model

Figure 7.16 : Visual Results of Oil Stains (Thick Bar) Defect Detection

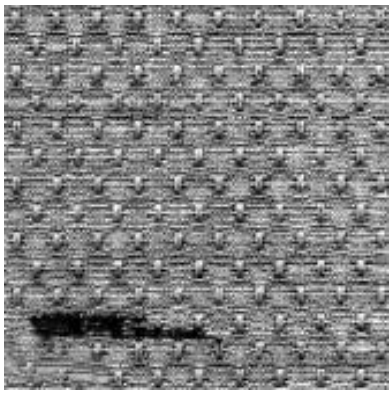

(a) Original

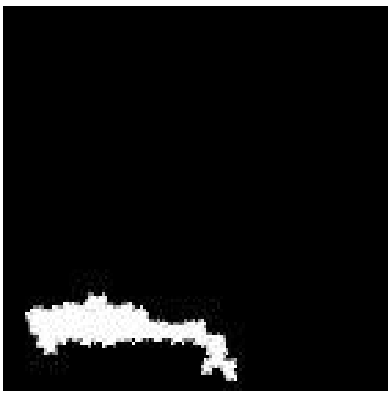

(b) WGIS Model

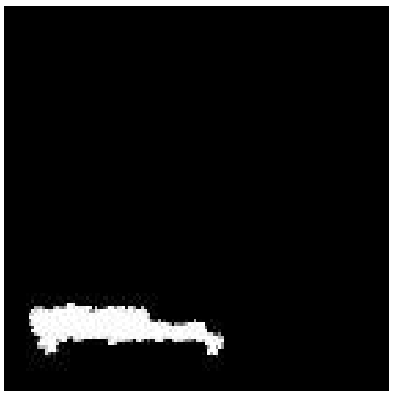

(c) GVPIN Model

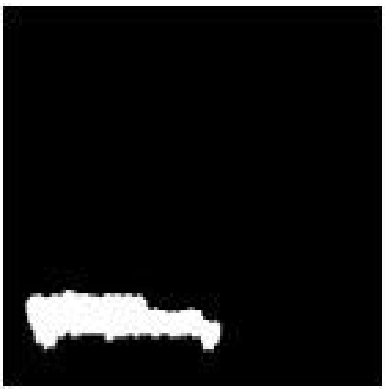

(d) MBM Model

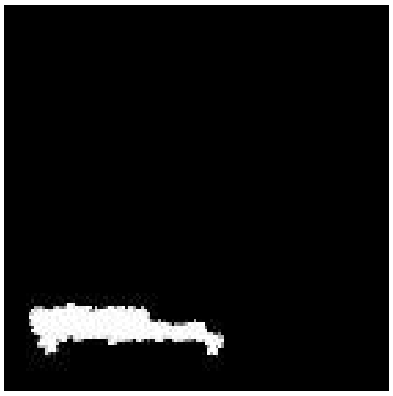

(e) EMBMAS Model

Figure 7.17 : Visual Results of Dirty Fabric (Thin Bar) Defect Detection